

Swings between rotation and accretion power in a millisecond binary pulsar

A. Papitto¹, C. Ferrigno², E. Bozzo², N. Rea¹, L. Pavan², L. Burderi³, M. Burgay⁴, S. Campana⁵,
T. Di Salvo⁶, M. Falanga⁷, M. D. Filipović⁸, P. C. C. Freire⁹, J. W. T. Hessels^{10,11}, A. Possenti⁴,
S. M. Ransom¹², A. Riggio³, P. Romano¹³, J. M. Sarkissian¹⁴, I. H. Stairs¹⁵, L. Stella¹⁶, D. F. Torres^{1,17},
M. H. Wieringa¹⁸ G. F. Wong^{8,14}

¹*Institute of Space Sciences (ICE; IEEC-CSIC), Campus UAB, Faculty of Science, Torre C5, parell, 2a planta, E-08193 Barcelona, Spain*

²*ISDC, Department of Astronomy, Université de Genève, chemin d'Écogia, 16, CH-1290 Versoix, Switzerland*

³*Dipartimento di Fisica, Università di Cagliari, SP Monserrato-Sestu, Km 0.7, I-09042 Monserrato, Italy*

⁴*INAF-Osservatorio Astronomico di Cagliari, loc. Poggio dei Pini, strada 54, I-09012 Capoterra, Italy*

⁵*INAF-Osservatorio Astronomico di Brera, Via Bianchi 46, I-23807 Merate, Lecco, Italy*

⁶*Dipartimento di Fisica e Chimica, Università di Palermo, via Archirafi 36, I-90123 Palermo, Italy*

⁷*International Space Science Institute, Hallerstrasse 6, CH-3012 Bern, Switzerland*

⁸*University of Western Sydney, Locked Bag 1797, Penrith South DC, NSW 1797, Australia*

⁹*Max-Planck-Institut für Radioastronomie, auf dem Hügel 69, 53121, Bonn, Germany*

¹⁰*ASTRON, the Netherlands Institute for Radio Astronomy, Postbus 2, 7990 AA, Dwingeloo, The Netherlands*

¹¹*Astronomical Institute “Anton Pannekoek”, University of Amsterdam, Science Park 904, 1098 XH Amsterdam, The Netherlands*

¹²*National Radio Astronomy Observatory (NRAO), 520 Edgemont Road, Charlottesville, VA 22901, USA.*

¹³*INAF-Istituto di Astrofisica Spaziale e Fisica Cosmica, Via U. La Malfa 153, I-90146 Palermo, Italy*

¹⁴*CSIRO Astronomy and Space Science, P.O. Box 76, Epping 1710, Australia*

¹⁵*Department of Physics and Astronomy, University of British Columbia, 6224 Agricultural Road, Vancouver, British Columbia V6T 1Z1, Canada*

¹⁶*INAF-Osservatorio Astronomico di Roma, Via di Frascati 33, I-00040 Monte Porzio Catone, Roma, Italy*

¹⁷*Institució Catalana de Recerca i Estudis Avançats (ICREA), 08010 Barcelona, Spain*

¹⁸*CSIRO Astronomy and Space Science, Locked Bag 194, Narrabri NSW 2390, Australia*

It is thought that neutron stars in low-mass binary systems can accrete matter and angular momentum from the companion star and be spun-up to millisecond rotational periods¹⁻³. During the accretion stage, the system is called a low-mass X-ray binary and bright X-ray emission is observed. When the rate of mass transfer decreases in the later evolutionary stages, these binaries host instead a radio millisecond pulsar^{4,5}, whose emission is powered by the neutron star’s rotating magnetic field⁶. This scenario is supported by the detection of X-ray millisecond pulsations from several accreting neutron stars^{7,8} and the evidence for a past accretion disc in a rotation-powered millisecond pulsar⁹. It has been proposed

that a rotation-powered pulsar may temporarily switch on¹⁰⁻¹² during periods of low mass inflow¹³ in some such systems. However, only indirect evidence for this transition had been observed¹⁴⁻¹⁸. Here we report the detection of accretion-powered, millisecond X-ray pulsations from a neutron star previously seen as a rotation-powered radio pulsar. Within a few days following a month-long X-ray outburst, radio pulses were again detected. This not only demonstrates the evolutionary link between accretion and rotation-powered millisecond pulsars, but also that some systems can swing between the two states on very short timescales.

The X-ray transient IGR J18245–2452 was first detected by INTEGRAL on 28 March 2013, and is located in the globular cluster M28. The X-ray luminosity of a few $\times 10^{36}$ erg s⁻¹ (0.3-10 keV), and the detection by the X-ray Telescope (XRT) on-board Swift of a burst originated by a thermonuclear explosion at the surface of the compact object¹⁹, firmly classified this source as an accreting neutron star with a low-mass companion. An observation performed by XMM-Newton on 4 April 2013 revealed a coherent modulation of its X-ray emission at a period of 3.93185 ms (see Fig. 1 and 2). We observed delays of the pulse arrival times produced by the orbit of the neutron star around a companion star of a mass $> 0.17 M_{\odot}$, with an orbital period of 11.0 hours (see Fig. 2). The spin and orbital parameters of the source were further improved by making use of a second XMM-Newton observation, as well as two observations performed by Swift/XRT (see Table 1).

Cross-referencing with the known rotation-powered radio pulsars in M28, we found that PSR J1824–2452I has ephemerides^{20,21} identical to those of IGR J18245–2452 (see Table 1). However,

the X-ray pulsations we have observed from IGR J18245–2452 are not powered by the rotation of the magnetic field as for the radio emission of PSR J1824–2452I. The pulse amplitude was observed to vary in strong correlation with the X-ray flux, implying that pulsations came from a source emitting $\approx 10^{36}$ erg s⁻¹ in X-rays; this value is larger by more than two orders of magnitudes than the luminosity shown by the X-ray counterparts of rotation-powered radio millisecond pulsars²², while it nicely agrees with the X-ray output of accretion-powered millisecond pulsars⁷. The X-ray spectrum of IGR J18245–2452 was also typical of this class, and the broad emission line observed at an energy compatible with the iron K- α transition (6.4–6.97 keV) is most easily interpreted in terms of reflection of hard X-rays by a truncated accretion disk²³. Furthermore, pulsations were detected by Swift-XRT during the decay of a thermonuclear burst, following a runaway nuclear burning of light nuclei accreted onto the neutron star surface. Such bursts are unambiguous indicators that mass accretion is taking place¹⁹, and the oscillations observed in some of them trace the spin period of the accreting neutron star²⁴.

We derived a precise position for IGR J18245–2452 using a Chandra image taken on 29 April 2013, while the source was fading in X-rays. Analysis of archival Chandra observations from 2008 indicate that IGR J18245–2452 already showed variations of its X-ray luminosity by an order of magnitude, as shown in Fig. 3, suggesting it underwent other episodes of mass accretion in the past few years. This 2008 enhancement of the X-ray emission followed the nearest previous detection of the radio pulsar, on 13 June 2008, by less than two months, indicating a very rapid transition from rotation to accretion-powered activity (see Table 3 in Supplementary Information for a summary of past observations of the source in the X-ray and radio band). The Chandra

position of IGR J18245–2452 is compatible with a variable unpulsed radio source that we have detected with the Australia Compact Telescope Array on 2013, April 5, with spectral properties typical of an accreting millisecond pulsar in outburst²⁵.

A combination of serendipitous and target-of-opportunity observations with the Green Bank Telescope (GBT), Parkes radio telescope, and Westerbork Synthesis Radio Telescope (WSRT) partially map the reactivation of IGR J18245–2452 as the radio pulsar PSR J1824–2452I (see Table 3 in Supplementary Information). No pulsed radio emission was seen in any of the three 2013 April observations, compatible with the neutron star being in an accretion phase and inactive as a radio pulsar. We caution however, that a non-detection of radio pulsations from PSR J1824–2452I can also be due to eclipsing and that the lack of observable radio pulsations does not necessarily prove the absence of an active radio pulsar mechanism^{20,22}. Radio pulsations were detected in 5 of the 13 observations conducted with GBT, Parkes, and WSRT in 2013 May. These observations demonstrate that the radio pulsar mechanism was active no more than a few weeks after the peak of the X-ray outburst.

In the last decade, IGR J18245–2452 has thus shown unambiguous tracers of both rotation and accretion powered activity, providing conclusive evidence for the evolutionary link between neutron stars in low mass X-ray binaries and millisecond radio pulsars. The source swung between rotation and accretion powered states on few-day to few-month time scales; this establishes the existence of an evolutionary phase during which a source can alternate between these two states over a time scale much shorter than the Gyr-long evolution of these binary systems, as they are

spun-up by mass accretion to millisecond spin periods²⁶. It is probable that a rotation powered pulsar switches on also during the X-ray quiescent states of other accreting millisecond pulsars^{14–18}, even if radio pulsations were not detected²⁷, so far.

The short time-scales observed for the transitions between accretion and rotation powered states of IGR J18245–2452 are comparable with those typical of X-ray luminosity variations. Like other X-ray transients, IGR J18245–2452 is X-ray bright ($L_X \approx 10^{36}$ erg s⁻¹) only during a few month-long periods called ‘outbursts’, while outside these episodes it spends years in an X-ray quiescent state ($L_X \lesssim 10^{32}$ erg s⁻¹). These variations are caused by swings of the mass in-flow rate onto the neutron star¹³, and our findings strongly suggest that this quantity mainly regulates the transitions between accretion and rotation powered activity, compatible with earlier suggestions^{5,10–12}. The X-ray luminosity of IGR J18245–2452 during quiescence ($L_X \approx 10^{32}$ erg s⁻¹) implies that rate of mass accretion was not larger than $\dot{M} \lesssim 10^{-14} M_\odot \text{ yr}^{-1}$, during such a state. The presence of radio millisecond pulsations indicates that the pulsar magnetosphere kept the plasma beyond the light cylinder radius (located at a distance of ≈ 200 km), despite the pressure exerted by the mass inflowing from the companion star. A pulsar magnetic field of the order of 10^8 – 10^9 G is able to satisfy this condition, and to explain the quiescent X-ray luminosity in terms of the pulsar rotational power (for a typical conversion efficiency of about 1%). The irregular disappearance of the radio pulses of PSR J1824–2452I during the rotation powered stage suggests that, during that phase, most of the matter that the companion transfers towards the neutron star is ejected by the pressure of the pulsar wind^{5,28}. A slight increase of the mass transfer rate may subsequently push the magnetosphere back inside the light cylinder¹². After a disk had sufficient time

to build up, an X-ray outburst is expected to take place, as in the case of IGR J18245–2452 during the observations reported here. As the mass accretion rate decreases during the decay of the X-ray outburst, the pressure of the magnetosphere is able to, at least partially, sweep away the residual matter from the surroundings of the neutron star, and a rotation-powered pulsed radio emission can reactivate. Our observations prove that such transitions can take place in both directions, on a time scale shorter than expected, perhaps only a few days.

The discovery of IGR J18245–2452, swinging between rotation and accretion-powered emission, represents the most stringent probe of the recycling scenario^{1–3}, and the existence of an unstable intermediate phase in the evolution of low mass X-ray binaries, offering the unprecedented opportunity to study in detail the transitions between these two states.

Acknowledgements This letter is based on ToO observations made by XMM-Newton, Chandra, INTEGRAL, Swift, ATCA, WSRT, GBT, and PKS. We thank the respective directors and operation teams for their support. Work done in the framework of the grants AYA2012-39303, SGR2009-811, and iLINK2011-0303, and with the support of CEA/Irfu, IN2P3/CNRS and CNES (France), INAF (Italy), NWO (The Netherlands), and NSERC (Canada). A. Pa. is supported by a Juan de la Cierva Research Fellowship. A. R. acknowledges Sardinia Regional Government for financial support (P.O.R. Sardegna ESF 2007-13). D. F. T was additionally supported by a Friedrich Wilhelm Bessel Award of the Alexander von Humboldt Foundation. L. P. thanks the Société Académique de Genève and the Swiss Society for Astrophysics and Astronomy. Finally, we acknowledge the use of data supplied by the UK Swift Science Data Centre at the University of Leicester. A. Pa. thanks S. Giannetti, D. Lai, R. V. E. Lovelace, M. M. Romanova for stimulating discussions, and Wolf Sol. Dig. for operational support.

Author Contributions A. Pa., C. F. and E. B. collected and analysed XMM-Newton data. A. Pa. and C. F. detected the pulsar in XMM-Newton data and derived its orbital solution. A. Pa. discovered the equivalence of its parameters with a radio pulsar, the thermonuclear burst and the burst oscillations. N. R. analysed Chandra data, detecting the X-ray quiescent counterpart of the source and past accretion events. L. P., M. H. W., M. D. F. and G. F. W. analysed ATCA data. E. B., S. C., P. R., A. Pa. and A. R. analysed Swift data. E. B. and C. F. analysed INTEGRAL data. J. W. T. H. analysed WSRT data. M. B. and J. M. S. analysed PKS data. J. W. T. H., S. M. R., A. Po. and I. H. S. and P. C. C. F. analysed GBT data. A. R. provided valuable software tools. A. Pa., N. R., and J. W. T. H. wrote the manuscript, with significant contribution by all the authors in interpreting the results and editing of the manuscript.

Competing Interests The authors declare that they have no competing financial interests.

Correspondence Correspondence and requests for materials should be addressed to A. Papitto (email: papitto@ice.csic.es).

Table 1: Spin and orbital parameters of IGR J18245–2452 and PSR J1824–2452I.

Parameter	IGR J18245–2452	PSR J1824–2452I
Right Ascension (J2000)	$18^h 24^m 32.53(4)^s$	
Declination (J2000)	$-24^\circ 52' 08.6(6)''$	
Reference epoch (MJD)	56386.0	
Spin period (ms)	3.931852642(2)	3.93185(1)
Spin period derivative	$< 1.3 \times 10^{-17}$	
RMS of pulse time delays (ms)	0.1	
Orbital period (hr)	11.025781(2)	11.0258(2)
Projected semi-major axis (lt-s)	0.76591(1)	0.7658(1)
Epoch of zero mean anomaly (MJD)	56395.216893(1)	
Eccentricity	$\leq 1 \times 10^{-4}$	
Pulsar mass function (M_\odot)	$2.2831(1) \times 10^{-3}$	$2.282(1) \times 10^{-3}$
Minimum companion mass (M_\odot)	0.174(3)	0.17(1)
Median companion mass (M_\odot)	0.204(3)	0.20(1)

Coordinates, spin, and orbital parameters of IGR J18245–2452=PSR J1824–2452I. Celestial coordinates of IGR J18245–2452 are derived from a Chandra X-ray observation performed using the High Resolution Camera (HRC-S) on 29 April 2013 (see Fig. 3). The spin and orbital parameters of IGR J18245–2452 were derived by modelling the pulse arrival time delays of the fundamental frequency component, as observed in the 0.5–10 keV energy band by the EPIC pn camera on-board XMM-Newton, and by the X-ray Telescope on-board Swift (see Fig. 2 and Supplementary Information for details). The solution covers the interval between 30 March and 13 April 2013. The peak-to-peak amplitude of the fundamental varied in correlation with the observed count rate (Spearman’s rank correlation coefficient of $\rho = 0.79$ for 45 points, which has a probability of less than 10^{-10} if the variables are uncorrelated) with a maximum of 18%. When detected, the second harmonic has an amplitude between 2 and 3%. The minimum and median mass of the companion star were evaluated for a $1.35 M_\odot$ mass of the neutron star, and inclination of the system of 90° and 60° , respectively. The spin and orbital parameters of PSR J1824–2452I were taken from ref. 20 and the ATNF pulsar Catalogue²¹, considering errors on the last significant digit there quoted. The numbers in parentheses represent the uncertainties on the respective parameter evaluated at a 1σ confidence level. Upper limits are quoted at a 3σ confidence level.

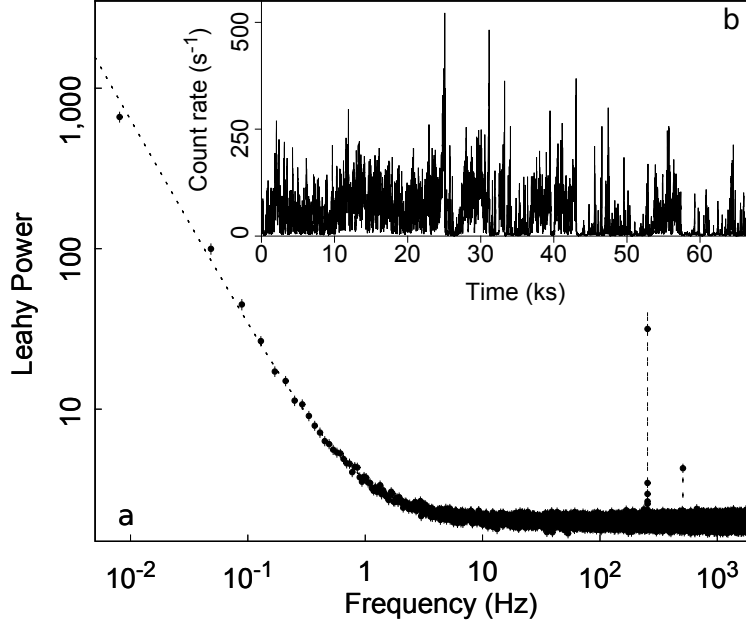


Figure 1: **Variability of the X-ray emission of IGR J18245–2452.** **a**, Fourier power spectral density of the 0.5–10 keV X-ray photons observed by the EPIC pn camera on-board XMM-Newton, during an observation starting on 13 April 2013, for an exposure of 67.2 ks (Obs. ID 0701981501). The power spectrum was obtained by sampling the light curve with a time binning of 0.236 ms, and averaging intervals of 128 s of length. The times of arrival of photons were converted to the barycentre of the Solar System and to the line of nodes of the binary system hosting IGR J18245–2452, by using the parameters listed in Table 1. The peaks at 254.3 and 508.6 Hz represent the first and second harmonic of the coherent modulation of the X-ray emission of IGR J18245–2452. Considering photons observed during a 2-ks interval, not corrected for the pulsar orbital motion, the signal at the spin period of the neutron star is detected at a significance $\gtrsim 80\sigma$. The dashed solid line is the sum of a power-law noise function, $P(f) \propto f^{-\gamma}$, with $\gamma = 1.291(4)$, and of a white noise spectrum with an average value of $1.9900(2) \text{ Hz}^{-1}$. Even considering the whole length of the time series, no break of the power-law noise could be detected at low frequencies. **b**, 0.5–10 keV light curve of the same observation, with a bin time of 5 s. The possibility of contamination by soft proton flares was ruled out by extracting a light curve from a background region observed by EPIC MOS cameras far from the source. Similar properties of variability than those shown here are observed during an XMM-Newton observation starting on 3 April 2013, for an exposure of 26.7 ks (Obs. ID 0701981401).

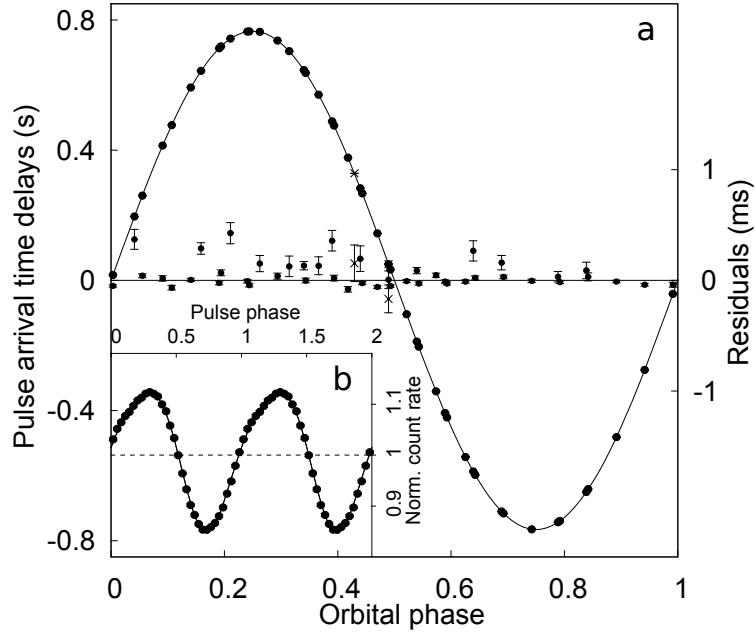


Figure 2: Spin and orbit of IGR J18245–2452. **a**, Pulse arrival time delays caused by the orbital motion of the neutron star (left axis) as measured by XMM-Newton during observations starting on 3 and 13 April 2013 (dots; Obs. ID 0701981401 and 0701981501, with exposure of 26.7 and 67.2 ks, respectively), and by Swift during observations starting on 30 March and 7 April 2013 (crosses; Obs. ID 00552369000 and 00032785005, with exposure of 0.6 and 1.6 ks, respectively). Residuals with respect to best fit timing solution (solid line) are also shown (right axis). Pulse profiles observed in 2 ks long intervals were modelled using $n = 12$ phase bins. The significance of each detection was assessed from the probability that the variance of each folded pulse profile were compatible with counting noise, assuming that in absence of any signal the latter is distributed as a chi-squared variable with $(n - 1)$ degrees of freedom²⁹. Only detections with a significance larger than 3σ were considered. Pulse arrival time delays were determined through standard methods of least square fitting of the pulse profiles²³, using two harmonic components and considering the values measured for the fundamental frequency component. **b**, Average pulse profile sampled in 32 phase bins, accumulated over the two XMM-Newton observations (black dots), and the best fit decomposition with two harmonics (solid line). The amplitude of the first and second harmonic was 13.4(1) and 1.9(1)%, respectively. Two cycles are plotted for clarity. In both panels, plotted error bars are the standard deviation of each measure.

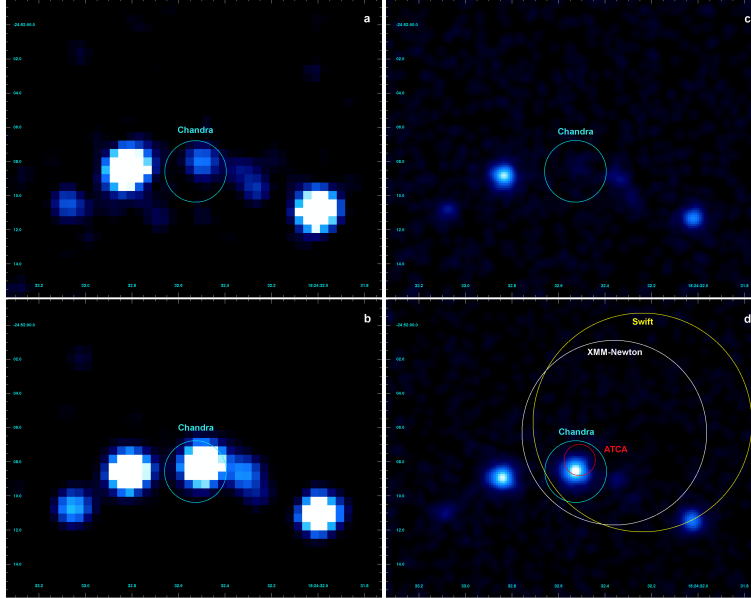


Figure 3: **Long term X-ray variability of IGR J18245–2452.** **a, b**, Chandra/ACIS-S images of the core of M28 taken during 4 August 2002, and 7 August 2008, respectively. **c, d**, Chandra/HRC-S images of the same field taken during 27 May 2006, and 29 April 2013, respectively. Images in the upper panels (**a, c**) shows the source in X-ray quiescence, emitting a luminosity of few $\times 10^{32}$ erg s^{-1} , while during observations of the lower panels (**b, d**) the X-ray luminosity was of few $\times 10^{33}$ erg s^{-1} (see Supplementary Information for details). The luminosity emitted during the 2013 observation (**d**) was three orders of magnitude lower than that observed by Swift (3.5×10^{36} erg s^{-1} on 30 March 2013) and XMM-Newton (1.1×10^{36} erg s^{-1} on 3 April 2013) at the onset of the X-ray outburst, compatible with the source being close to the end of the accretion episode. A distance³⁰ of 5.5 kpc was considered to derive these estimates. During the 2013 outburst, the 0.5-10 keV spectrum of IGR J18245–2452 is dominated by a ≈ 1.4 power law interpreted as Comptonization in an optically thin medium, of seed photons with a temperature of ≈ 0.3 keV. XMM-Newton observations also detected a thermal component, modelled as an accretion disc truncated at an apparent projected inner radius of ≈ 50 km, and a broad line, modelled with a Gaussian centred at 6.74 ± 0.11 keV and of 1.1 ± 0.2 keV of width, compatible with iron K- α transition (see Supplementary Information for details). The plotted error circles represent the 3σ confidence level position of IGR J18245–2452, derived by Chandra (29 April 2013), XMM-Newton EPIC-MOS (3 and 13 April 2013), Swift XRT (30 March 2013), and ATCA (5 April 2013), plotted as a cyan, white, yellow and red circles, respectively.

Supplementary Information

1 INTEGRAL detection of IGR J18245–2452

IGR J18245–2452 was first detected³¹ by the hard X-ray imager IBIS³² using the ISGRI³³ detector on-board INTEGRAL³⁴, on 28 March 2013, during observations of the Galactic Center. We analysed the corresponding data (pointings from 83 to 107 in satellite revolution 1276) by using the Off-line Science Analysis software provided by the Integral Science Data Centre. The source was detected in the ISGRI mosaicked image at a significance level of 21σ in the 20–40 keV energy band and 15σ in the 40–80 keV energy band (see Figure 4). The best source position was obtained at RA=276.14°, Dec=24.88° (J2000), with an associated uncertainty of 1.4' at 90% confidence level, well within the globular cluster M28. During the first detection of the source, its flux estimated from the ISGRI data was 9×10^{-10} erg cm⁻² s⁻¹ in the 20-100 keV energy band, during an effective exposure time of 32 ks, corresponding to a luminosity of 3×10^{36} erg s⁻¹, at a distance³⁰ of 5.5 kpc. The source was outside the field of view of the JEM-X instrument³⁵, sensitive in the 3–30 keV energy band, during the entire observation.

2 XMM-Newton observations of IGR J18245–2452

Following the detection of IGR J18245–2452 by INTEGRAL, we obtained two target of opportunity observations with the X-ray Multi-Mirror Mission³⁶ (*XMM-Newton*), starting on 3 April 2013, at 23:49 (Obs. ID 0701981401, OBS 1, hereafter) and 13 April at 06:25 (Obs. ID 0701981501, OBS 2), and lasting 26.7 and 67.2 ks, respectively (all the epochs are given in the Coordinated

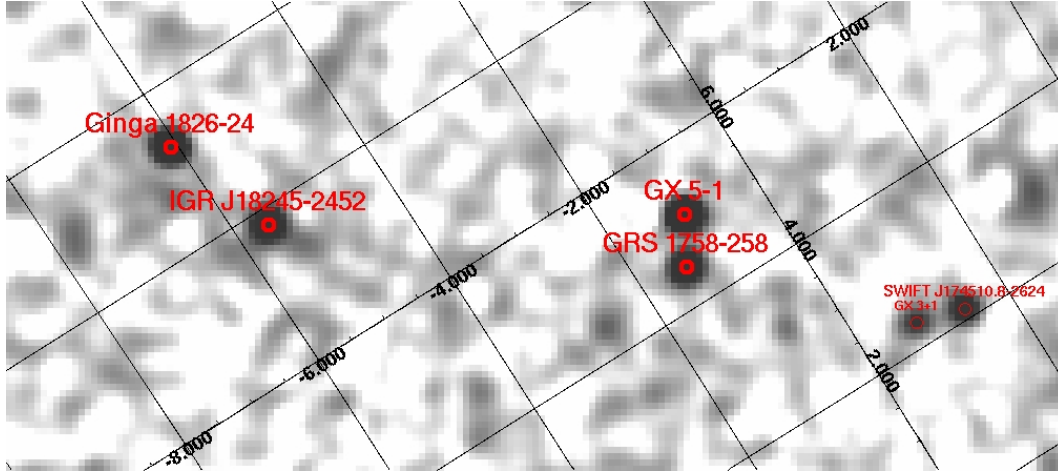


Figure 4: Mosaic of the IBIS/ISGRI field of view around IGR J18245–2452 obtained by using Science Windows 83-107 collected in the direction of the source during satellite revolution 1276 (20–40 keV energy range).

Universal Time). The European Photon Imaging Camera (EPIC) pn³⁷ was operated in fast timing mode, the two EPIC MOS cameras³⁸ in small window imaging mode, and the Reflection Grating Spectrometers³⁹ (RGS) in standard spectroscopy mode. A thick blocking filter was used to shield the EPIC cameras from contamination of optical light. All the data were reduced by using the latest version of the XMM-Newton Science Analysis Software (SAS ver. 13). The average count rates observed by the EPIC pn, EPIC MOS1, EPIC MOS2, RGS1 and RGS2 (in their first order of dispersion) during the first (second) observations were 68.1 (71.0), 11.8 (11.7), 11.6 (11.5), 0.68 (0.86) and 0.69 (0.88) s⁻¹, respectively. Since the source is detected also at energy larger than 10 keV, we built a 0.5–10 keV light curve from a background region falling in one of the outer chips of the EPIC MOS cameras which was not pointing the source, in order to ensure that soft proton flares of Solar origin did not contaminate the observations.

Timing Analysis. The timing observing mode of the EPIC pn camera has a timing resolution of $29.52 \mu\text{s}$. This resolution is achieved by losing spatial information along one of the axes of the CCD. To extract the source emission, we considered X-ray photons falling within $86.1''$ from the source position measured along one of the pointing axes (corresponding to a full width of 21 EPIC pn pixels), and containing 95% of the energy at every observed wavelength. The background emission was extracted from a region of width $12''$ (corresponding to 3 EPIC pn pixels).

Although X-ray pulsations from several accreting millisecond pulsars have already been observed by XMM-Newton^{23,40–43}, this is the first time that pulsations from an accreting millisecond pulsar have been discovered by this observatory. In order to perform a timing analysis of the signal, the times of arrival of X-ray photons were converted to the Solar System barycentre, by using the position determined by Chandra (see Sec. 4 below) and Solar System ephemerides JPL DE405. We derived a zeroth order orbital solution by measuring the spin period in 2-ks long intervals through an epoch folding technique²⁹, and modelling the orbital modulation affecting the values obtained. To assess the significance of any detection we considered that in the absence of any periodic signal, the variance of a folded profile follows a χ^2_{n-1} distribution with $n - 1$ degrees of freedom, where n is the number of phase bins used to sample the signal period²⁹ ($n = 12$ in this case). We then used the preliminary determination of the pulsar orbital parameters to convert the photon arrival times to the line of nodes of the binary system. This procedure was iterated until the spin period was observed to be constant throughout the observations. To further refine the parameters, we then folded data around the current best estimate of the spin period, considering 12 phase bins and describing the pulse profile with two harmonic components. The variation of the phase of the first harmonic

over time was modelled in terms of the difference between the orbital and spin parameters used to correct the photon arrival times, and the actual ones⁴⁴. The procedure was iterated until no significant corrections to the parameters were found within the uncertainties¹⁸. We checked that the phase difference between the first and second harmonic component was compatible with a constant.

The amplitude of the harmonic component at the fundamental frequencies varied between 18% and the non detection, in strong positive correlation with the count rate observed in the 0.5–10 keV (see Figure 5). The Spearman’s rank correlation coefficient evaluated from the observed count rate and amplitude is $\rho = 0.79$ for 45 points, implying a probability of less than 10^{-10} that the two variables are not correlated.

Spectral Analysis. We built an X-ray spectrum of the emission observed by the EPIC pn by excluding the two brightest columns of CCD pixels (RAWX=37–38), to avoid the effect of photon pile up during the time intervals in which the count rate was the highest. Spectral bins were grouped to over-sample the effective instrument resolution by a factor not larger than three. Response matrices were built following the guidelines provided by the XMM-Newton calibration technical notes. The two observations were modelled simultaneously as they had a compatible average spectral shape. We modelled the 0.6–11 keV observed spectra with an accretion disk spectral component⁴⁵ (`diskbb` in the terminology used by the spectral fitting routine used, Heasarc’s XSPEC v.12.8.0), and with the emission produced by a thermal distributions of electrons which Compton up-scatter soft seed X-ray photons, with a black-body spectral shape^{46,47} (`nthcomp`). A similar spectral decomposition well described the X-ray spectra shown by accreting millisecond

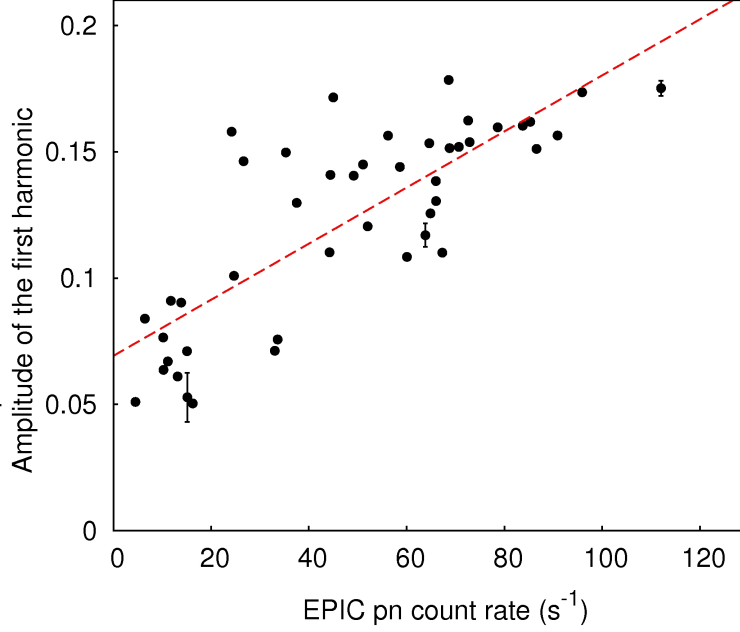


Figure 5: Peak-to-peak amplitude of the first harmonic measured during XMM-Newton OBS 1 and OBS 2, normalised to the average count rate, and 0.5-10 keV EPIC pn count rate evaluated over 2 ks long intervals. The dashed red line is the best fit linear regression between the two variables. Typical errors bars are shown for sample points.

pulsars⁴⁸, observed by the EPIC pn camera^{23,40-43}. The temperature of the electron cloud was fixed at 50 keV, outside the energy band observed by the EPIC pn camera, following the values usually observed at higher energies from accreting millisecond pulsars^{48,49} ($kT_e \gtrsim 20$ keV). Absorption of the interstellar medium was modelled according to the Tuebingen-Boulder model (Wilms, J. et al. 2011, in preparation, <http://pulsar.sternwarte.uni-erlangen.de/wilms/research/tbabs/>). The value of the absorption column was fixed to the value measured by fitting the average spectra observed by the RGS 1 and 2 with an absorbed power law ($N_H = 0.31(1) \times 10^{22} \text{ cm}^{-2}$); solar abundances were considered. A broad Gaussian emission feature centred at an energy compatible with iron K- α emission (6.4–6.97 keV), and a narrow emission feature most probably

due to calibration residuals around the edge of Au (Guainazzi, M. et al. 2012, available from <http://xmm2.esac.esa.int/docs/documents/CAL-TN-0083.pdf>), decreased significantly the variance of model residuals. The best-fit parameters obtained modelling the spectra observed during the two XMM-Newton are given in Table 2, while the observed spectrum and residuals are plotted in Figure 6.

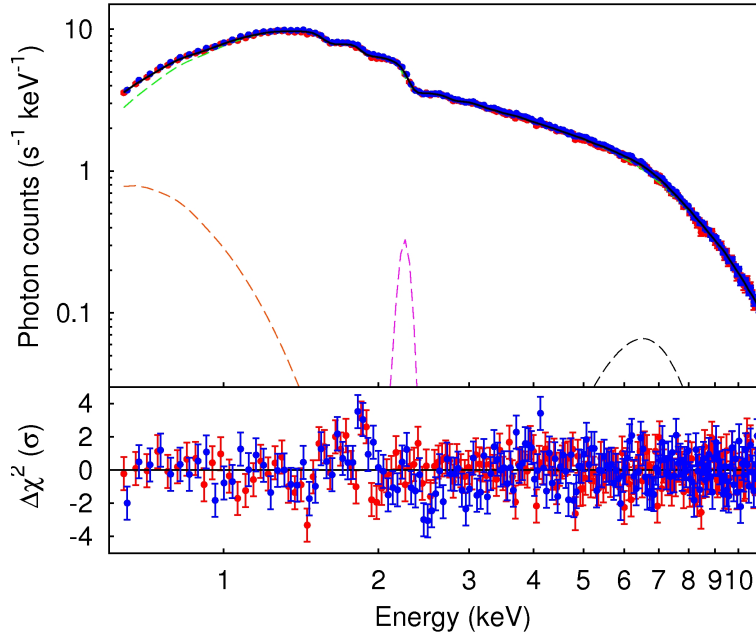


Figure 6: X-ray spectrum observed by the EPIC pn camera during OBS 1 and OBS 2 (red and blue points, respectively). The best fit model is plotted as a black solid line, the disc emission, the Comptonized emission, the iron emission feature, and the feature of calibration origin, are plotted as an orange, green, grey and magenta dashed lines, respectively (top panel). Residuals in units of σ of the observed spectra, with respect to the best fit model (bottom panel).

Table 2: Average spectral parameters of IGR J18245–2452.

Absorption column ($N_{\text{H}}^{(a)}$)	$0.31(1) \times 10^{22} \text{ cm}^{-2}$
Inner disk temperature (kT_{in})	0.13(1) keV
Apparent inner disk radius ($R_{\text{in}}\sqrt{\cos i}^{(b)}$)	$52_{-13}^{+19} \text{ km}$
Seed photon temperature (kT_{soft})	0.31(1) keV
Asymptotic power-law photon index (Γ)	1.41(1)
Electron temperature (kT_{e})	50 keV
Energy of iron line (E_{Fe})	$6.74 \pm 0.11 \text{ keV}$
Width (σ_{Fe})	1.1(2) keV
Normalisation (N_{Fe})	$4.8(1) \times 10^{-3} \text{ cm}^{-2} \text{ s}^{-1}$
Energy of line of calibration origin (E_{cal})	2.24(1) keV
Normalisation (N_{cal})	$1.3(2) \times 10^{-4} \text{ cm}^{-2} \text{ s}^{-1}$
Unabsorbed flux (0.5–10 keV; F_1) ^(c)	$3.08(1) \times 10^{-10} \text{ erg cm}^{-2} \text{ s}^{-1}$
Unabsorbed flux (0.5–10 keV; F_2) ^(d)	$3.17(1) \times 10^{-10} \text{ erg cm}^{-2} \text{ s}^{-1}$
Reduced chi-squared, $\chi_{\nu}^2(\text{d.o.f.})$	1.27(355)

Parameters based on spectral modelling of the two observations of IGR J18245–2452 performed by the EPIC pn camera. Values in parentheses are the uncertainties on the last significant digit, evaluated at a 90% confidence level.

^(a) The value of the interstellar absorption column density was measured by modelling the spectra observed by the two units of the RGS with an absorbed power law. This value was held fixed when fitting the EPIC pn spectra. We used abundances and photoelectric cross-sections from ref. 54 and 55, respectively.

^(b) The disk apparent radius depends on the disk inclination, i , and was evaluated for a distance of 5.5 kpc (ref. 35).

^(c–d) Unabsorbed flux during OBS 1 and OBS 2, respectively.

The position. To determine the source position we accumulated images from the EPIC MOS1 and MOS 2 in the energy bands 0.5-1 keV, 1-2 keV, 2-4.5 keV, and 4.5-12 keV, during the time intervals in which the source count rate was $< 1.5 \text{ s}^{-1}$ (0.5–10 keV). This selection prevented pile-up and resulted in a total effective exposure time of 5.7 and 13.8 ks for the two instruments in OBS 1 and OBS 2, respectively. We created an exposure map using the attitude information to mask out the regions of the detector where not enough exposure was available, and performed a first localisation of the sources in the raw images using the sliding box method⁵⁰. A background map was then produced from the previous images by removing the identified sources (taking into account the local instrument point spread function), and used together with previous products to perform a second optimised source localisation. The data of the two MOS cameras in the two observations and different energy bands provided a total of 16 independent estimates of the source position. By averaging such estimates we obtained a position of RA=18^h24^m32.36^s Dec=−24°52′06.3″. We added in quadrature the 1σ uncertainty we derived with the described analysis (1.5″) to the systematic error reported in the XMM catalogue⁵⁰ (1.0″), to obtain a total uncertainty of 1.8″ (1σ confidence level). The error circle at a 3σ confidence level is plotted as a white circle in Fig. 3 of the main body of the Letter.

3 Swift observations of IGR J18245–2452

After the initial arc-second localisation with the X-ray Telescope⁵¹ (XRT) on-board Swift⁵², the source triggered the Burst Alert Telescope⁵³ (BAT) on 30 April 2013 at 02:22:21 UT and subsequently at 15:10:37 UT and 15:17:33.61 UT. Several observations with XRT were obtained start-

ing from 30 April, including a intensive one between the BAT triggers (Obs. Id 32787) and a long term one (Obs. Id 32785). Analysis of the XRT observation performed on 30 April yielded a determination⁵⁴ of the position of the source RA=18^h24^m32.24^s Dec=−24°52′05.7″, with an uncertainty of 3.5″ at a 90% confidence level, compatible with that determined by ref. 59, and those measured by EPIC MOS (see Sec.2 above), Chandra (see Sec. 4 below), and ATCA (see Sec. 5). The 0.5–10 keV flux corrected for absorption attained a maximum level of $9.6(1) \times 10^{-10}$ erg cm^{−2} s^{−1} during an observation starting on 30 March 2013 (Obs.ID 00552369000), with a spectral distribution well described by a power law with index $\Gamma = 1.35 \pm 0.04$. The last detection was obtained during a 0.8-ks observation performed on 1 May 2005 (Obs. ID 00032785021), with an observed flux of $(1.6 \pm 0.4) \times 10^{-12}$ erg cm^{−2} s^{−1}. This value of the flux was estimated assuming a $\Gamma = 2.5 \pm 0.6$, power-law shaped spectrum, as derived summing all Swift observations taken in the week starting from 21 April 2013. We note that a flux contamination of $\approx 3 \times 10^{-13}$ erg cm^{−2} s^{−1} is expected to be produced by other unresolved source in M28, among which PSR B1821-24 gives the largest contribution^{22,56}. Details of a sample of Swift/XRT observations are given in Supplementary Table 4.

During an observation that started on 7 April at 20:32 (Obs. ID 00032785005), a bursting event was observed^{43,57} by the XRT when it was observing in windowed timing mode with a temporal resolution of 1.78 ms. The burst profile has the typical shape observed from thermonuclear explosions taking place at the surface of the neutron star¹⁹, with a fast rise of $\lesssim 10$ s and an exponential decay on a time scale of 38.9 ± 0.5 s (see red dashed line in Figure 7). We performed a time resolved analysis of the emission observed by XRT during the burst. We fit all spectra with a black

body emission absorbed by the interstellar medium, fixing the value of the absorption column to that indicated by the XMM-Newton analysis (see Tab. 2). We used the emission observed by XRT during a 100-s interval before the burst as a background to the burst emission. The values of temperature we observed are plotted as blue dots in Figure 7. The temperature decay observed during the burst tail agrees with the cooling expected after the thermonuclear burning¹⁹, confirming the nature of the observed event.

We used the Chandra pulsar position (see Sec. 4, below) and orbital parameters determined from the XMM-Newton observations (see Sec.2 and Table 1 in the main body of the Letter) to report the photons arrival times to the Solar system Barycentre and to the pulsar line of nodes. We divided the first 160 s since the burst onset into four intervals, finding in the second one a significant signal at the pulsar period, with an amplitude of $13 \pm 2\%$ (see the inset of Figure 7). After taking into account the number of trials made, the detection is significant at a 3.2σ level. A signal with an amplitude of $6.0 \pm 1.2\%$ is detected during the 740 s observed by XRT before the burst onset. The increase of the signal amplitude indicates that the signal observed during the burst is related to this event (i.e., it is a burst oscillation⁵⁸) and is not coming from a background source present within the field of view of XRT. Similar results were reported by ref. 65 and 66.

We also searched for oscillations during the other observations performed by Swift, and found a signal significant above a 3σ confidence level during the observation starting on 30 March 2013 (Obs. ID 00552369000), with an amplitude of $7.4 \pm 1.9\%$.

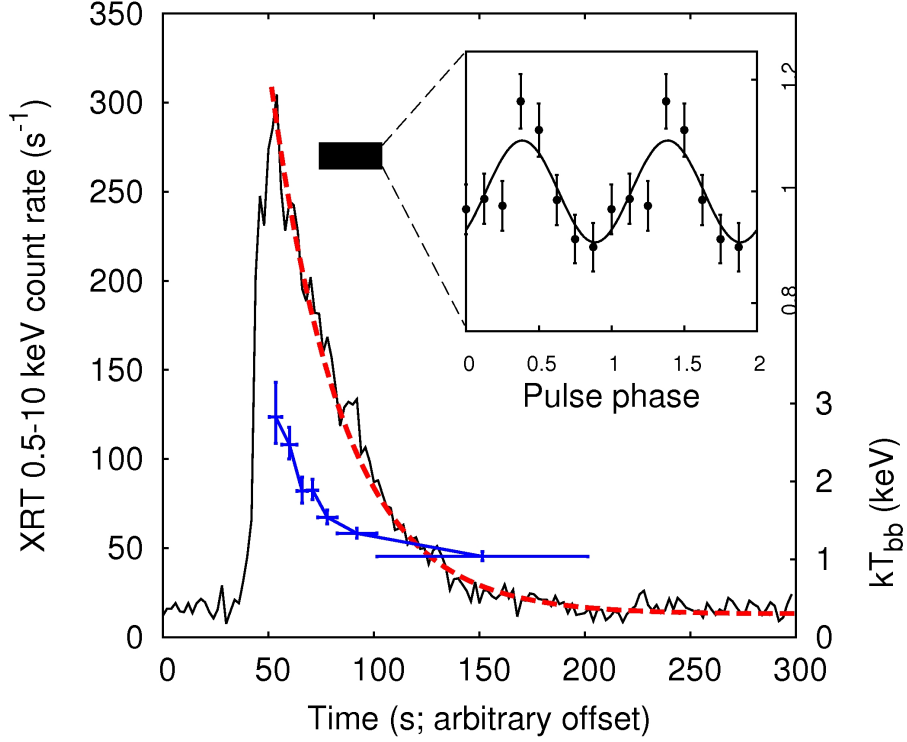


Figure 7: Thermonuclear burst observed by XRT, with the best fit exponential decay model plotted as a red dashed line. Blue points show the temperature of the black body which we used to model the XRT 0.5-10 keV spectra, and refer to the right axis. The inset shows the pulse profile observed at the spin period of the source, during the interval marked by the horizontal thick bar.

4 Chandra observations of IGR J18245–2452

The *Chandra* X-ray observatory observed IGR J18245–2452 on 29 April 2013, starting from 00:24:14 for 53 ks, via Director’s Discretionary Time. The observations were performed using the High Resolution Camera⁶¹ (HRC–S) in timing mode, which has a $6'' \times 30''$ field of view with a $16\text{-}\mu\text{s}$ timing resolution, but no spectral information. Data were reduced with the CIAO 4.5 software. We first checked the data for the presence of solar flares and extracted a new observation-specific

bad-pixel file. We then ran a degap correction, and cleaned the image for the hot pixels.

The new Chandra image of the M28 globular cluster was compared to the several observations of the field performed by Chandra during the past decade (see Table 3 for a complete list, and Fig. 3 of the main body of the Letter for a comparison). We identified one source (source 23 from ref. 60) to be an order of magnitude brighter than in many previous Chandra observations. We used the CIAO tools `wavdetect` and `celldetect` to infer a good position for the transient source, which was $RA=18^h 24^m 32.527^s$, $Dec=-24^\circ 52' 08.58''$, with $0.6''$ uncertainty (at $1-\sigma$ confidence level, inferred from a $0.3''$ and a $0.5''$ statistical and pointing accuracy, respectively). The position of this transient source is consistent within a $3-\sigma$ confidence level with the XMM–Newton (see Sec. 2), Swift (see Sec. 3) and ATCA position (see Sec. 5 below) of IGR J18245–2452 (see Fig. 3 of the main body of the Letter). We therefore identify it as the accreting X-ray pulsar, IGR J18245–2452.

We have extracted the source events from a $2''$ region around the position of the source (and background spectra far from the globular cluster). In this Chandra observation the source had a count rate of 0.0251(5) counts per second (see Tab. 3), which assuming the spectral shape that IGR J18245–2452 had in the closest Swift XRT observation (a power-law with $\Gamma = 2.5 \pm 0.6$; derived summing all Swift observations taken in the week starting from 21 April 2013), leads to a 0.5–10keV observed flux $\sim 4 \times 10^{-13} \text{ erg cm}^{-2} \text{ s}^{-1}$.

We searched for a coherent signal at the spin period of the source in the time series corrected for the spacecraft and orbital motion, and converted to the Solar System Barycentre. No signal was

detected at a confidence level of 3σ , with an upper limit of 17% on the pulse amplitude, derived following the prescription given by Vaughan et al. [65]. Pulsations at an amplitude lower than such a value were observed during most of the XMM-Newton observations (see Figure 5), when the source was brighter by three orders of magnitude. The non-detection of pulsations does not rule out that the X-ray emission of IGR J18245–2452 was pulsed during the Chandra observation, at a level similar to that previously seen.

We have re-analysed all archival observations performed by Chandra in the past decade to identify and follow the flux evolution of the source. Timing and spectral data were always extracted from a $2''$ region around the position of the source. A previous X-ray outburst of IGR J18245–2452 is detected during the August 2008 observations performed with the Advanced CCD Imaging Spectrometer⁶² (ACIS; see Fig. 3 of the main body of the Letter). The light curve of this previous outburst shows a strong variability on many timescales (see Figure 8). The most noticeable event is a total quenching of the X-ray emission for a timescale of ~ 10 hrs, compatible with a complete orbital period. We did not detect a significant energy dependency of the light curve shape.

Spectra were extracted from all the archival observations performed with ACIS-S (all taken in VFaint mode), which have a good spectral and imaging resolution, but a 3.2 s timing resolution, insufficient to search for millisecond pulsations. We found a good fit ($\chi^2_\nu = 0.91$ with 378 degrees of freedom) when modelling all ACIS-S spectra together with an absorbed power-law model (leaving the photoelectric absorption parameter, N_H , tied to be the same for all spectra). We found a flux variability of more than one order of magnitude between the 2002 and the 2008 observations

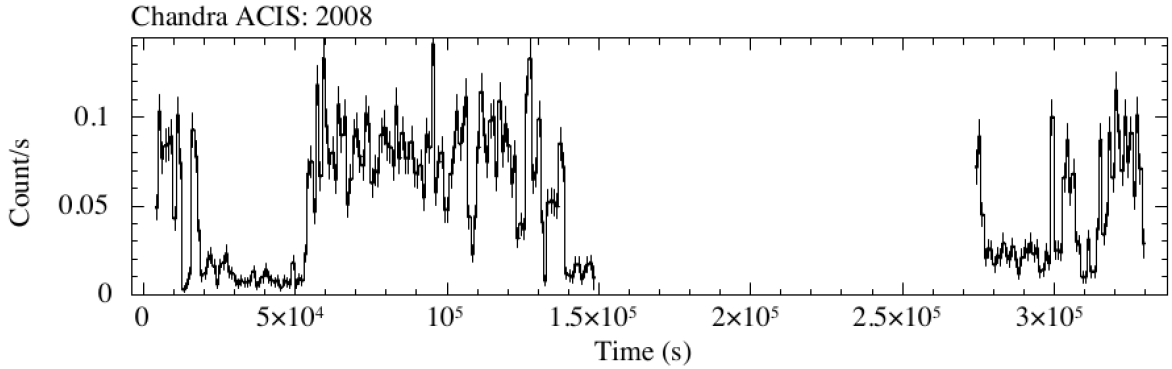


Figure 8: Chandra ACIS-S light curve of the August 2008 observations, when the source was undergoing an X-ray outburst. Light curve is background subtracted, binned at 1000s and in the 0.3–10 keV energy range. Data were not available during the interval between 1.5×10^5 and 2.7×10^5 s, since the beginning of the first observation.

of IGR J18245–2452 (see Figure 9 and Tab. 3). In particular, we found $N_H = 0.26(2) \times 10^{22} \text{ cm}^{-2}$ (with abundances and photoelectric cross-sections from ref. 69 and 70, respectively), a stable photon index $\Gamma \sim 1.5$, and a 0.5–10 keV flux varying from 2.4 to $64 \times 10^{-14} \text{ erg cm}^{-2} \text{ s}^{-1}$ (all errors are at 90% confidence level).

5 ATCA observations of IGR J18245–2452

On 2013 April 5 we observed IGR J18245–2452 with the Australia Telescope Compact Array (ATCA), at 9 and 5.5 GHz simultaneously. The data were analysed with the Miriad package distributed by ATNF⁶⁵. Only one source was detected in the inner core of the cluster, at a significance level of nearly 20σ in both frequencies, allowing for an accurate determination of its position at $\text{RA}=18^{\text{h}}24^{\text{m}}32.51^{\text{s}}$ $\text{Dec}=-24^{\circ}52'07.9''$, with a 90% confidence error of $0.5''$. This position is con-

Table 3: *Chandra* observations of the Globular Cluster M28.

Instrument	ObsID	Date	Exposure time (ks)	Source Count/s ^a	Γ^b	Flux ^c
ACIS-S	2684	2002-07-04	12.7	0.0029(6)	1.5(0.7)	3.1(9)
ACIS-S	2685	2002-08-04	13.5	0.0030(5)	1.4(0.7)	3.5(9)
ACIS-S	2683	2002-09-09	14.1	0.0025(4)	1.6(0.7)	2.4(7)
HRC-S	2797	2002-11-08	48.3	0.0036(5)	1.5 fix	4.8
HRC-S	6769	2006-05-27	40.9	0.0036(5)	1.5 fix	4.8
ACIS-S	9132	2008-08-07	142.3	0.0563(6)	1.51(5)	64(2)
ACIS-S	9133	2008-08-10	54.5	0.04393(9)	1.58(7)	47(2)
HRC-S	15645	2013-04-29	53.0	0.0503(8)	2.5 fix	41

^a We report the HRC-S counts converted in ACIS-S counts for an easier comparison. The HRC-S original count rate is 0.0012(3) for the first and second HRC-S observation, and 0.0251(5) for the more recent one.

^b Absorption column density is $N_H = 0.26(2) \times 10^{22} \text{ cm}^{-2}$.

^c Absorbed, in the 0.5–10 keV energy range, and in units of $10^{-14} \text{ erg cm}^{-2} \text{ s}^{-1}$. HRC-S fluxes are estimated assuming the source N_H and a power-law spectrum with $\Gamma = 2.5$.

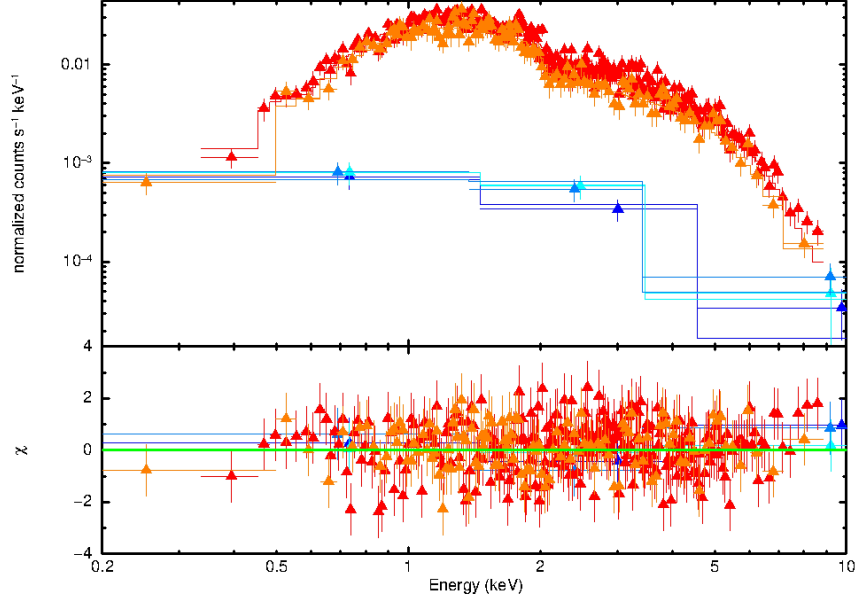


Figure 9: ACIS–S spectra of all *Chandra* observations of IGR J18245–2452 (4 July 2002, cyan triangles; 4 August 2002, light blue triangles; 9 September 2002, blue triangles; 7 August 2008, red triangles; 10 August 2008, orange triangles; see Supplementary Table 2 for details) modelled with an absorbed power-law model (top panel) and residuals with respect to the best fitting absorbed power-law model (bottom panel).

sistent with that determined by *Chandra* (see Sec. 4 and Fig. 3 of the main body of the Letter). The mean flux density of this source was 0.75 ± 0.04 (0.62 ± 0.03) mJy at 9 (5.5) GHz respectively, yielding a mean spectral index of 0.4 ± 0.2 . During the first 90 minutes of the observation, the source was strongly variable, reaching up to 2.5 times the mean flux density.

The spectral properties of the ATCA source are similar to those observed from other accreting millisecond pulsars²⁵, and interpreted in terms of emission originating from shocks within material ejected by the X-ray pulsar. Besides PSR J1824–2452I=IGR J18245–2452, which was powered by accretion at that moment, none of the other rotation-powered pulsars in the cluster were detected

during the ATCA observation.

6 Parkes radio telescope observations of PSR J1824–2452I

IGR J18245–2452 was observed three times with the 64-m Parkes radio telescope in 2013 April/May (see Supplementary Table 4). We used the position determined by Chandra (see Sec. 4 above). The observations were carried out using simultaneously the Berkeley-Parkes Swinburne Recorder (BPSR) and the Parkes Digital Filterbank (PDFB4) in search mode, for the first epoch, and BPSR and the analogue filterban (AFB), for the subsequent ones. The backends were operating at central frequencies of 1382 MHz (BPSR) and 1369 MHz (PDFB4 and AFB) , over bandwidths of 400 and 256 MHz respectively, subdivided in 1024 frequency channels (512 for AFB). The total usable bandwidth for BPSR, after removal of a known interference from the Thuraya3 satellite, is 350 MHz.

The resulting time series, 2-bit sampled every $64 \mu\text{s}$ for BPSR and PDFB4, and 1-bit sampled every $80 \mu\text{s}$ for AFB, were folded with the `dspsr` package⁶⁶ using the X-ray ephemeris presented in this work and using a value of the dispersion measure²⁰ of 119 pc cm^{-3} . PSR J1824–2452I was detected in two of three Parkes observations (see Supplementary Table 4). In the case of the non-detection, the flux density upper limit derived using the radiometer equation modified for pulsars⁶⁷ is $S_{min} = 0.067 \text{ mJy}$ for a signal with a signal-to-noise ratio $\text{SNR}=8$ and a pulse duty cycle of 15 per cent. We caution that Parkes non-detection, as well as other radio non-detections presented below, cannot be taken as strong evidence that the radio pulsar was not active. PSR

J1824–2452I is well known to eclipse in the radio²², particularly around superior conjunction, and this is likely the cause of at least some of the radio non-detections presented in Supplementary Table 4. Though there is no published flux density for PSR J1824–2452I, given its comparable brightness to other pulsars in M28, it is likely that if the source was emitting as a radio pulsar during these observations that it would be at the threshold of detectability during this 64-m Parkes radio telescope observation - especially if the signal was further perturbed by intra-binary material, as in similar systems. Therefore, we consider these observations only moderately constraining as to whether the source was emitting as a radio pulsar at this epoch.

7 Westerbork Synthesis radio telescope observations of PSR J1824–2452I

We observed IGR J18245–2452 during four sessions in 2013 May using the Westerbork Synthesis radio telescope (WSRT). The pointing position was $18^h 24^m 32.496^s$, $24^\circ 52'07.799''$. We used WSRT in the tied-array mode (gain, $G = 1.2$ K/Jy), combining 13 of the individual 25-m dishes in phase and recording with the PuMaII pulsar data recorder⁶⁸. We recorded a 160-MHz bandwidth and coherently de-dispersed and folded the data offline using the `dspsr` package⁶⁶ and the X-ray-derived ephemeris presented here. PSR J1824–2452I was just barely detected in one of four WSRT observations (see Supplementary Table 4). Using the radiometer equation modified for pulsar signals⁶⁷, we can place a flux density limit of $S_{1400} = 0.08$ mJy on radio emission from the pulsar in the case of the non-detections. Note that the flux of PSR J1824–2452I is very close to WSRT’s detection threshold and, as mentioned above, the radio pulsar may simply have been eclipsed in the case of non-detections.

8 Green Bank Telescope observations of PSR J1824–2452I

We observed IGR J18245–2452 during seven sessions in 2013 May using the Green Bank Telescope (GBT). The Chandra position presented here was used for pointing, and data were acquired using the GUPPI data recorder⁶⁹ in a 800-MHz band centered at 2.0GHz. PSR J1824–2452I was detected in two of seven observations (see Supplementary Table 4). Flux density limits in the case of non-detections are $S_{2000} \lesssim 20\mu\text{Jy}$, but come with the same caveats about eclipsing as described above. Supplementary Table 4 also lists a number of archival detections of PSR J1824–2452I with the GBT since its discovery²⁰ as a radio pulsar in 2006. These observations have been acquired as part of a regular timing program of the radio pulsars in M28 (Ransom et al.) and together with archival X-ray observations they conclusively demonstrate that the system has switched between rotation-powered radio pulsar and accretion-powered X-ray pulsar (and back) during 2006–2013.

Table 4: **Abridged Radio/X-ray History of PSR J1824–2452I/IGR J18245–2452**: Flux densities of radio observations were measured at 2.0 GHz (GBT), 1.4 GHz (WSRT/Parkes), and 5.5/9 GHz (ATCA). Radio non-detections are marked by a dash in the flux column, and are only moderately constraining as to whether the source was emitting as a radio pulsar at this epoch (see text for details). GBT non-detections prior to 2012-10-07 are not listed. Observed X-ray fluxes are evaluated in the 0.5–10 keV band (20–100 keV for INTEGRAL), and given in mCrab ($1\text{Crab} = 4.32 \times 10^{-8} \text{ erg cm}^{-2} \text{ s}^{-1}$ in the 0.5–10 keV band).

UT Date	MJD Start	Telescope	Type	Flux	Comments
2002-07-04	52,459.752	Chandra/ACIS-S	X-rays	$(7 \pm 2) \times 10^{-4}$ mCrab	X-ray Quiescence
2002-08-04	52,490.990	Chandra/ACIS-S	X-rays	$(8 \pm 2) \times 10^{-4}$ mCrab	X-ray Quiescence
2002-09-09	52,526.705	Chandra/ACIS-S	X-rays	$(6 \pm 2) \times 10^{-4}$ mCrab	X-ray Quiescence
2002-11-08	52,586.237	Chandra/HRC-S	X-rays	1×10^{-3} mCrab	X-ray Quiescence
2006-01/02	53,738 – 53,781	GBT	Radio		Discovery of PSR J1824–2452I (ref. 69)
2006-05-27	53,882.520	Chandra/HRC-S	X-rays	1×10^{-3} mCrab	X-ray Quiescence
2006/2007		Various GBT	Radio Observations		
2007-12-30	54,464.746	GBT	Radio	$\sim 20 \mu\text{Jy}$	Radio Pulsations
2008-04-17	54,573.354	GBT	Radio	$\sim 20 \mu\text{Jy}$	Radio Pulsations
2008-06-13	54,631.274	GBT	Radio	$\sim 20 \mu\text{Jy}$	Radio Pulsations

Continued on next page

Table 4 – continued from previous page

UT Date	MJD Start	Telescope	Type	Flux	Comments
2008-08-07	54,685.865	Chandra	X-rays	$(14.8 \pm 0.5) \times 10^{-3}$ mCrab	X-ray Enhanced
2008-08-10	54,688.993	Chandra	X-rays	$(10.9 \pm 0.5) \times 10^{-3}$ mCrab	X-ray Enhanced
2009-05-06	54,957.418	GBT	Radio	$\sim 20 \mu\text{Jy}$	Radio Pulsations
2009/2012		Various GBT Radio Observations			
2012-10-07	56,207.967	GBT	Radio	–	–
2013-01-06	56,298.702	GBT	Radio	–	–
2013-03-28	56,379.122	INTEGRAL/ISGRI	X-rays	~ 90 mCrab	Discovery of IGR J18245–2452
2013-03-30	56,381.632	Swift/XRT	X-rays	(19.4 ± 0.2) mCrab	X-ray Outburst / Pulsations
2013-04-04	56,386.018	XMM-Newton/EPIC pn	X-rays	(6.56 ± 0.02) mCrab	X-ray Outburst / Pulsations
2013-04-05	56,387.720	ATCA	Radio	(0.62 ± 0.03) mJy (5.5 GHz)	Non-pulsed
				(0.75 ± 0.04) mJy (9 GHz)	Non-pulsed
2013-04-08	56,390.481	GBT	Radio	–	–
2013-04-13	56,395.294	XMM-Newton/EPIC pn	X-rays	(6.76 ± 0.02) mCrab	X-ray Outburst / Pulsations
2013-04-15	56,397.469	GBT	Radio	–	–
2013-04-29	56,411.010	Chandra/HRC-S	X-rays ^a	9.5×10^{-3} mCrab	X-ray Enhanced
2013-04-29	56,411.560	Parkes	Radio	–	–

Continued on next page

Table 4 – continued from previous page

UT Date	MJD Start	Telescope	Type	Flux	Comments
2013-05-01	56,413.557	Swift/XRT	X-rays ^{a,b}	$(3.8 \pm 1.0) \times 10^{-2}$ mCrab	Latest X-ray detection
2013-05-02	56,414.164	WSRT	Radio	$50 \pm 30 \mu\text{Jy}$	Radio Pulsations
2013-05-04	56,416.162	WSRT	Radio	–	–
2013-05-06	56,418.170	WSRT	Radio	–	–
2013-05-06	56,418.296	GBT	Radio	–	–
2013-05-06	56,418.831	Swift/XRT	X-rays ^{a,b}	$< 4 \times 10^{-2}$ mCrab	X-ray non detection
2013-05-07	56,419.114	WSRT	Radio	–	–
2013-05-09	56,421.442	GBT	Radio	–	–
2013-05-10	56,422.544	Parkes	Radio	$60 \pm 30 \mu\text{Jy}$	Radio Pulsations
2013-05-11	56,423.405	GBT	Radio	$10 \pm 5 \mu\text{Jy}$	Radio Pulsations
2013-05-13	56,425.432	GBT	Radio	$20 \pm 10 \mu\text{Jy}$	Radio Pulsations
2013-05-13	56,425.684	Parkes	Radio	$50 \pm 30 \mu\text{Jy}$	Radio Pulsations
2013-05-18	56,430.277	GBT	Radio	–	–
2013-05-24	56,436.437	GBT	Radio	–	–
2013-05-31	56,443.183	GBT	Radio	–	–

^a Flux estimated assuming a $\Gamma = 2.5$ power-law spectral shape. ^b Other unresolved sources^{2,56} in M28 are expected to give a contribution of

$\approx 7 \times 10^{-3}$ mCrab to the quoted flux value/upper limit. Upper limits are evaluated at 3- σ confidence level.

1. Bisnovatyi-Kogan, G. S. & Komberg, B. V. Pulsars and close binary systems. *Sov. Astron.* **18**, 217 (1974).
2. Alpar, M. A., Cheng, A. F., Ruderman, M. A. & Shaham, J. A new class of radio pulsars. *Nature* **300**, 728–730 (1982).
3. Radhakrishnan, V. & Srinivasan, G. On the origin of the recently discovered ultra-rapid pulsar. *Curr. Sci. India* **51**, 1096–1099 (1982).
4. Backer, D. C., Kulkarni, S. R., Heiles, C., Davis, M. M. & Goss, W. M. A millisecond pulsar. *Nature* **300**, 615–618 (1982).
5. Ruderman, M., Shaham, J. & Tavani, M. Accretion turnoff and rapid evaporation of very light secondaries in low-mass X-ray binaries. *Astrophys. J.* **336**, 507–518 (1989).
6. Pacini, F. Energy Emission from a Neutron Star. *Nature* **216**, 567–568 (1967).
7. Wijnands, R. & van der Klis, M. A millisecond pulsar in an X-ray binary system. *Nature* **394**, 344–346 (1998).
8. Chakrabarty, D. & Morgan, E. H. The two-hour orbit of a binary millisecond X-ray pulsar. *Nature* **394**, 346–348 (1998).
9. Archibald, A. M. *et al.* A Radio Pulsar/X-ray Binary Link. *Science* **324**, 1411–1414 (2009).
10. Stella, L., Campana, S., Colpi, M., Mereghetti, S. & Tavani, M. Do quiescent soft X-ray transients contain millisecond radio pulsars? *Astrophys. J.* **423**, L47–L50 (1994).

11. Campana, S., Colpi, M., Mereghetti, S., Stella, L. & Tavani, M. The neutron stars of Soft X-ray Transients. *Astron. Astrophys. Rev.* **8**, 279–316 (1998).
12. Burderi, L. *et al.* Where May Ultrafast Rotating Neutron Stars Be Hidden? *Astrophys. J.* **560**, L71–L74 (2001).
13. van Paradijs, J. On the Accretion Instability in Soft X-Ray Transients. *Astrophys. J.* **464**, L139–L141 (1996).
14. Burderi, L., Di Salvo, T., D’Antona, F., Robba, N. R. & Testa, V. The optical counterpart to SAX J1808.4-3658 in quiescence: Evidence of an active radio pulsar? *Astron. and Astrophys.* **404**, L43–L46 (2003).
15. Hartman, J. M. *et al.* The Long-Term Evolution of the Spin, Pulse Shape, and Orbit of the Accretion-powered Millisecond Pulsar SAX J1808.4-3658. *Astrophys. J.* **675**, 1468–1486 (2008).
16. Di Salvo, T., Burderi, L., Riggio, A., Papitto, A. & Menna, M. T. Orbital evolution of an accreting millisecond pulsar: witnessing the banquet of a hidden black widow? *Mon. Not. R. Astron. Soc.* **389**, 1851–1857 (2008).
17. Patruno, A. The Accreting Millisecond X-ray Pulsar IGR J00291+5934: Evidence for a Long Timescale Spin Evolution. *Astrophys. J.* **722**, 909–918 (2010).
18. Papitto, A. *et al.* Spin down during quiescence of the fastest known accretion-powered pulsar. *Astron. Astrophys.* **528**, A55 (2011).

19. Lewin, W. H. G., van Paradijs, J. & Taam, R. E. X-Ray Bursts. *Sp. Sc. Rev.* **62**, 223–389 (1993).
20. Bégin, S. *A search for fast pulsars in globular clusters*. Master of science, The Faculty of Graduate Studies (Physics), The University of British Columbia (2006).
21. Manchester, R. N., Hobbs, G. B., Teoh, A. & Hobbs, M. The Australia Telescope National Facility Pulsar Catalogue. *Astron. J.* **129**, 1993–2006 (2005).
22. Bogdanov, S. *et al.* Chandra X-ray Observations of 12 Millisecond Pulsars in the Globular Cluster M28. *Astrophys. J.* **730**, 81 (2011).
23. Papitto, A. *et al.* XMM-Newton detects a relativistically broadened iron line in the spectrum of the ms X-ray pulsar SAX J1808.4-3658. *Astron. Astrophys.* **493**, L39–L43 (2009).
24. Chakrabarty, D. *et al.* Nuclear-powered millisecond pulsars and the maximum spin frequency of neutron stars. *Nature* **424**, 42–44 (2003).
25. Gaensler, B. M., Stappers, B. W. & Getts, T. J. Transient Radio Emission from SAX J1808.4-3658. *Astrophys. J.* **522**, L117–L119 (1999).
26. Bhattacharya, D. & van den Heuvel, E. P. J. Formation and evolution of binary and millisecond radio pulsars. *Phys. Rep.* **203**, 1–124 (1991).
27. Burgay, M. *et al.* A Search for Pulsars in Quiescent Soft X-Ray Transients. I. *Astrophys. J.* **589**, 902–910 (2003).

28. Fruchter, A. S., Stinebring, D. R. & Taylor, J. H. A millisecond pulsar in an eclipsing binary. *Nature* **333**, 237–239 (1988).
29. Leahy, D. A., Elsner, R. F. & Weisskopf, M. C. On searches for periodic pulsed emission - The Rayleigh test compared to epoch folding. *Astrophys. J.* **272**, 256–258 (1983).
30. Harris, W. E. A Catalog of Parameters for Globular Clusters in the Milky Way. *Astron. J.* **112**, 1487–1488 (1996).
31. Eckert, D. *et al.* IGR J18245-2452: a new hard X-ray transient discovered by INTEGRAL. *Astron. Tel.* **4925**, 1 (2013).
32. Ubertini, P. *et al.* IBIS: The Imager on-board INTEGRAL. *Astron. and Astrophys.* **411**, L131–L139 (2003).
33. Lebrun, F. *et al.* ISGRI: The INTEGRAL Soft Gamma-Ray Imager. *Astron. and Astrophys.* **411**, L141–L148 (2003).
34. Winkler, C. *et al.* The INTEGRAL mission. *Astron. Astrophys.* **411**, L1–L6 (2003).
35. Lund, N. *et al.* JEM-X: The X-ray monitor aboard INTEGRAL. *Astron. and Astrophys.* **411**, L231–L238 (2003).
36. Jansen, F. *et al.* XMM-Newton observatory. I. The spacecraft and operations. *Astron. and Astrophys.* **365**, L1–L6 (2001).
37. Strüder, L. *et al.* The European Photon Imaging Camera on XMM-Newton: The pn-CCD camera. *Astron. and Astrophys.* **365**, L18–L26 (2001).

38. Turner, M. J. L. *et al.* The European Photon Imaging Camera on XMM-Newton: The MOS cameras : The MOS cameras. *Astron. and Astrophys.* **365**, L27–L35 (2001).
39. den Herder, J. W. *et al.* The Reflection Grating Spectrometer on board XMM-Newton. *Astron. and Astrophys.* **365**, L7–L17 (2001).
40. Gierliński, M. & Poutanen, J. Physics of accretion in the millisecond pulsar XTE J1751-305. *Mon. Not. R. Astron. Soc.* **359**, 1261–1276 (2005).
41. Patruno, A. *et al.* SAXJ1808.4-3658: high-resolution spectroscopy and decrease of pulsed fraction at low energies. *Mon. Not. R. Astron. Soc.* **396**, L51–L55 (2009).
42. Papitto, A. *et al.* The X-ray spectrum of the newly discovered accreting millisecond pulsar IGR J17511-3057. *Mon. Not. R. Astron. Soc.* **407**, 2575–2588 (2010).
43. Papitto, A. *et al.* The accretion flow to the intermittent accreting millisecond pulsar, HETE J1900.1-2455, as observed by XMM-Newton and RXTE. *Mon. Not. R. Astron. Soc.* **429**, 3411–3422 (2013).
44. Deeter, J. E., Boynton, P. E. & Pravdo, S. H. Pulse-timing observations of Hercules X-1. *Astrophys. J.* **247**, 1003–1012 (1981).
45. Makishima, K. *et al.* Simultaneous X-ray and optical observations of GX 339-4 in an X-ray high state. *Astrophys. J.* **308**, 635–643 (1986).

46. Zdziarski, A. A., Johnson, W. N. & Magdziarz, P. Broad-band γ -ray and X-ray spectra of NGC 4151 and their implications for physical processes and geometry. *Mon. Not. R. Astron. Soc.* **283**, 193–206 (1996).
47. Życki, P. T., Done, C. & Smith, D. A. The 1989 May outburst of the soft X-ray transient GS 2023+338 (V404 Cyg). *Mon. Not. R. Astron. Soc.* **309**, 561–575 (1999).
48. Gierliński, M., Done, C. & Barret, D. Phase-resolved X-ray spectroscopy of the millisecond pulsar SAX J1808.4-3658. *Mon. Not. R. Astron. Soc.* **331**, 141–153 (2002).
49. Falanga, M. *et al.* INTEGRAL and RXTE observations of accreting millisecond pulsar IGR J00291+5934 in outburst. *Astron. Astrophys.* **444**, 15–24 (2005).
50. Watson, M. G. *et al.* The XMM-Newton serendipitous survey. V. The Second XMM-Newton serendipitous source catalogue. *Astron. and Astrophys.* **493**, 339–373 (2009).
51. Burrows, D. N. *et al.* The Swift X-Ray Telescope. *Sp. Sc. Rev.* **120**, 165–195 (2005).
52. Gehrels, N. *et al.* The Swift Gamma-Ray Burst Mission. *Astrophys. J.* **611**, 1005–1020 (2004).
53. Barthelmy, S. D. *et al.* The Burst Alert Telescope (BAT) on the SWIFT Midex Mission. *Sp. Sc. Rev.* **120**, 143–164 (2005).
54. Romano, P. *et al.* Swift observations of IGR J18245-2452. *Astron. Tel.* **4929**, 1 (2013).
55. Heinke, C. O., Bahramian, A., Wijnands, R. & Altamirano, D. IGR J18245-2452 is a new transient located in the core of the globular cluster M28. *Astron. Tel.* **4927**, 1 (2013).

56. Becker, W. *et al.* Chandra X-Ray Observatory Observations of the Globular Cluster M28 and Its Millisecond Pulsar PSR B1821-24. *Astrophys. J.* **594**, 798–811 (2003).
57. Linares, M. IGR J18245-2452: an accreting neutron star and thermonuclear burster in M28. *Astron. Tel.* **4960**, 1 (2013).
58. Watts, A. L. Thermonuclear Burst Oscillations. *Annu. Rev. Astron. Astr.* **50**, 609–640 (2012).
59. Patruno, A. Burst oscillations in the X-ray binary IGR J18245-2452 in M28. *Astron. Tel.* **5068**, 1 (2013).
60. Riggio, A. *et al.* Coherent pulsations and burst oscillations in the millisecond pulsar IGR J18245-2452/PSR J1824-2452I in M28. *Astron. Tel.* **5086**, 1 (2013).
61. Zombeck, M. V. *et al.* High-resolution camera (HRC) on the Advanced X-Ray Astrophysics Facility (AXAF). In *Society of Photo-Optical Instrumentation Engineers (SPIE) Conference Series, Vol. 2518* (1995).
62. Garmire, G. P., Bautz, M. W., Ford, P. G., Nousek, J. A. & Ricker, G. R., Jr. Advanced CCD imaging spectrometer (ACIS) instrument on the Chandra X-ray Observatory. In *Society of Photo-Optical Instrumentation Engineers (SPIE) Conference Series, Vol. 4851* (2003).
63. Anders, E. & Grevesse, N. Abundances of the elements - Meteoritic and solar. *Geochim. Cosmochim. A.* **53**, 197–214 (1989).
64. Balucinska-Church, M. & McCammon, D. Photoelectric absorption cross sections with variable abundances. *Astrophys. J.* **400**, 699–700 (1992).

65. Sault, R., Teuben, P. & Wright, M. A retrospective view of miriad. *ASP Conf. Ser.* **77**, 433–436 (1995).
66. van Straten, W. & Bailes, M. DSPSR: Digital Signal Processing Software for Pulsar Astronomy. *Publ. Astr. Soc. Austr.* **28**, 1–14 (2011).
67. Dewey, R. J., Taylor, J. H., Weisberg, J. M. & Stokes, G. H. A search for low-luminosity pulsars. *Astrophys. J.* **294**, L25–L29 (1985).
68. Karuppusamy, R., Stappers, B. & van Straten, W. PuMa-II: A Wide Band Pulsar Machine for the Westerbork Synthesis Radio Telescope. *Publ. Astr. Soc. Pac.* **120**, 191–202 (2008).
69. DuPlain, R. *et al.* Launching GUPPI: the Green Bank Ultimate Pulsar Processing Instrument. In *Society of Photo-Optical Instrumentation Engineers (SPIE) Conference Series*, vol. 7019 of *Society of Photo-Optical Instrumentation Engineers (SPIE) Conference Series* (2008).